Ultrafast Pump–Probe Spectroscopy of Native Etiolated Oat Phytochrome†

Sergei Savikhin,‡ Todd Wells,§ Pill-Soon Song,*,§ and Walter S. Struve*,‡

Department of Chemistry and Ames Laboratory—USDOE, Iowa State University, Ames, Iowa 50011, and Department of Chemistry and Institute for Cellular and Molecular Biology, University of Nebraska—Lincoln, Lincoln, Nebraska 68588-0304

Received March 11, 1993; Revised Manuscript Received May 12, 1993

ABSTRACT: Absorption difference profiles were obtained at wavelengths from 640 to 700 nm with 1–2-ps resolution in a study of primary photoprocesses in the Pr → Pfr transformation in native oat phytochrome. These experiments were performed using low-intensity laser pulses at high repetition rate; fast sample recycling ensured that essentially all phytochrome species were excited from the Pr ground state. The Pr*-stimulated emission decay at wavelengths >670 nm exhibits major components with lifetimes of ~16 and 50–60 ps. Formation of the asymptotic 695-nm lumi-R absorption spectrum rapidly follows stimulated emission decay. Photoexcitation of one or both of the lumi-R intermediates instantaneously recreates fluorescing Pr* phytochrome, which is spectroscopically and kinetically indistinguishable from that generated by direct illumination of ground-state Pr. This is consistent with assignment of lumi-R as a species in which the chromophore has isomerized from the Z,Z,Z to the Z,Z,E conformation. Anisotropy studies indicate that the orientations of the Pr and lumi-R absorption transition moments are nearly parallel, since little anisotropy decay occurs during the 500-ps time window of these experiments.

The excited-state kinetics and dark reactions associated with phototransformations of the plant chromoprotein phytochrome have attracted considerable interest (Linschitz et al., 1966; Cross et al., 1968; Braslavsky et al., 1980; Shimizaki et al., 1980; Cordonnier et al., 1981; Song et al., 1981, 1986; Holzwarth et al., 1984; Ruzsicska et al., 1985; Brock et al., 1987). This photoreceptor in green plants mediates the regulation of some 200 biological responses, including biosynthesis of chlorophylls, carotenoids, rubisco, and thylakoid membranes. Undegraded phytochrome from etiolated oat seedling shoots comprises a 124-kDa protein, to which a single open tetrapyrrole chromophore is covalently linked through Cys-321 (Hershey et al., 1985). At physiological temperatures, phytochrome exists in two stable forms. The inactive, red-absorbing form (Pr) exhibits an absorption band maximum at 665 nm ($\epsilon_{max} \sim 1.2 \times 10^5$ M^{-1} cm^{-1}; Litts et al., 1983). The band maximum of the active, far-red-absorbing Pfr form that controls developmental and morphogenic processes is situated at 730 nm (Zhang et al., 1992). The Pr and Pfr forms are reversibly interconverted by irradiation in their red and far-red absorption bands, respectively.

Following the seminal flash photolysis experiments of Linschitz et al. (1966), several groups have confirmed that the overall Pr → Pfr transformation includes a number of dark reactions, involving at least four intermediates (Cordonnier et al., 1981; Ruzsicska et al., 1985) and possibly five (Zhang et al., 1992). Two of these [termed lumi-R_1 and lumi-R_2 by Zhang et al. (1992), or I'_{700} and I''_{700} by Ruzsicska et al. (1985)] exhibit temperature-dependent microsecond lifetimes. At least two others [designated meta-Ra_1 and meta-Ra_2 by Zhang et al., (1992)] persist for several milliseconds to tens of milliseconds. While considerable agreement exists concerning the empirical lifetimes yielded by analyses of time-resolved absorption spectra for red-illuminated Pr oat phytochrome (Cordonnier et al., 1981; Ruzsicska et al., 1985; Zhang et al., 1992), the complexity of the Pr → Pfr kinetic scheme has so far precluded determination of its topology. In the most recent study by Zhang et al. (1992), global analyses of the observed spectral evolution were consistent with at least three distinct kinetic models. These included a fully sequential scheme (Pr* → lumi-R_1 → lumi-R_2 → meta-Ra_1 → meta-Ra_2 → meta-Rc → Pfr) and two other schemes, combining sequential and parallel dark reactions, in which separate kinetic branches are created by Pr* decay into lumi-R_1 and lumi-R_2.

The decay kinetics of Pr* phytochrome, whose 690-nm fluorescence band is readily monitored in time-correlated single photon counting experiments, have been extensively studied. One of the earliest fluorescence experiments was reported by Holzwarth et al. (1984). Triexponential models were required to fit Pr* decays from native 124-kDa oat phytochrome. The dominant component exhibited a lifetime of 48 ± 3 ps (typically with >90% of the preexponential factors); minor components were found with lifetimes of ~200 ps and ~1 ns. Essentially identical results were found in large (114, 118 kDa) and small (60 kDa) photochromes (Wendler et al., 1984). Brock et al. (1987) later characterized similar fluorescence decays for 124-kDa oat phytochrome in PBEG/H_2O at 293 K. The fast-component lifetime (34 ± 1 ps) exhibited little discernible isotope effect in PBEG/D_2O; the slowest component showed a substantial isotope effect (1040 and 1450 ps in PBEG/H_2O and PBEG/D_2O respectively). Song et al. (1989) studied effects of the chromophore environment microviscosity on Pr* fluorescence decays for 124-kDa oat phytochrome excited at 637 nm. The fast-component lifetime at 670-nm emission wavelength varied from 30.8 ps in phosphate buffer to 61.1 ps in 67% glycerol. Time-resolved fluorescence anisotropies at 660 and 700 nm exhibited an initial value $r(0) \sim 0.38$, and showed little decay [$r(t) > 0.36$] during the first few tens of picoseconds.

Photon counting studies with improved time resolution have recently uncovered the presence of an additional, ultrafast Pr* fluorescence component (Hermann et al., 1990; Holzwarth et al., 1992). In KPH buffer, this component exhibits lifetimes of 4–6 and 6–18 ps for 620- and 660-nm excitation wavelengths, respectively (Holzwarth et al., 1992). This is accompanied

† This research was supported by the donors of the Petroleum Research Fund, administered by the American Chemical Society (to W.S.S.), by the USPHS, NIH (GM36956, to P.-S.S.), and by the Army Research Office (28748-LS-SM, to P.-S.S.).

‡ Iowa State University.

§ University of Nebraska—Lincoln.

0006-2960/93/0432-7512$04.00/0

by a second Pr* fluorescence component, whose lifetime (42–54 ps in KPH) is similar to that of the fastest component observed under lower resolution in the earlier experiments. These two emission components have been attributed to the presence of two distinct, equilibrated Pr* states.

The time scale for lumi-R formation from electronically excited Pr* phytochrome is less well established. The early experiments of Linschitz et al. (1966) fixed an upper limit of ~100 μs for the rise time of an intermediate exhibiting an absorption band maximum at 695 nm. Subsequent experiments under nanosecond resolution also revealed instrument-limited rise times for the lumi-R_1 and lumi-R_2 transients, refining the upper limit to 50–60 ns (Cordonnier et al., 1981; Ruzsicska et al., 1985). In a picosecond transient absorption study, Lippitsch et al. (1988) excited Pr phytochrome at 621 nm with 6-ps laser pulses. The absorption difference spectrum between 600 and 700 nm was dominated during the first few tens of picoseconds by photobleaching of the Pr ground-state spectrum, and exhibited a maximum at ~670 nm. An absorption transient subsequently developed at ~690 nm; this was assigned to the lumi-R intermediate(s) previously observed in the flash photolysis experiments (Linschitz et al., 1966; Braslavsky et al., 1980; Shimizaki et al., 1981; Cordonnier et al., 1981) and low-temperature absorption studies (Cross et al., 1968; Song et al., 1981). The 665-nm photobleaching reportedly exhibited biexponential rise behavior, with lifetimes of ~5 and ~35 ps. The latter lifetime resembles that of a Pr* fluorescence component (Holzwarth et al., 1984; Brock et al., 1987; Wendler et al., 1984; Song et al., 1989). The 690-nm absorption feature assigned to lumi-R subsequently evolved with ~60-ps rise kinetics, leading Lippitsch et al. to conclude that the Pr* state does not decay directly into lumi-R. In their scenario, the Pr* state decayed with lifetime ~40 ps into a previously undetected intermediate ("prelumi-R") which then formed lumi-R phytochrome with ~60-ps kinetics.

These results contrast with more recent work by Kandori et al. (1992), who reported that excitation of large Pr phytochrome causes essentially instantaneous photobleaching of the Pr absorption spectrum, followed by formation of a 695-nm lumi-R absorption band with 24-ps kinetics. Since these somewhat resemble the Pr* fast-component lifetimes reported by most groups prior to the experiments of Hermann et al. (1990) and Holzwarth et al. (1992), it was inferred that the lumi-R state is formed *directly* upon decay of the Pr* state.

The presence of long-lived intermediates in the Pr → Pfr transformation complicates its investigation by ultrafast transient absorption spectroscopy. The use of unamplified, synchronously pumped dye lasers with a 76-MHz repetition rate offers high S/N (and therefore reliable extraction of multiple lifetime components) in pump–probe experiments. However, their 13-ns laser pulse spacing ensures that phytochrome intermediates (rather than ground-state Pr) will dominate the absorption of pump pulses, unless special precautions are taken for sample recirculation. The use of amplified dye laser pulses at lower repetition rates, combined with the use of broadband continuum pulses to probe transient absorption spectra, obviates this problem at the expense of lower S/N in time-resolved decays. The latter approach also raises issues of sample saturation and multiphotonic excitation. In this work, we report a pump–probe study of undegraded oat phytochrome based on the former technique. A novel centrifugal sample cell permits rapid recirculation of only ~0.2 mL of sample, ensuring that ground-state Pr phytochrome predominates in the absorption of ~40-pJ excitation pulses even at a 76-MHz repetition rate. Our qualitative results resemble those of Kandori et al. much more closely than those of Lippitsch et al. However, analyses of our absorption difference kinetics reveal that they contain multiple lifetime components similar to the ones found by Holzwarth et al. (1992). Our ability to spin the centrifugal cell at variable speed yielded unexpected dividends, since effects of incomplete sample recirculation could be studied. This has in turn illuminated the relationship between the Pr* state and the lumi-R intermediate(s).

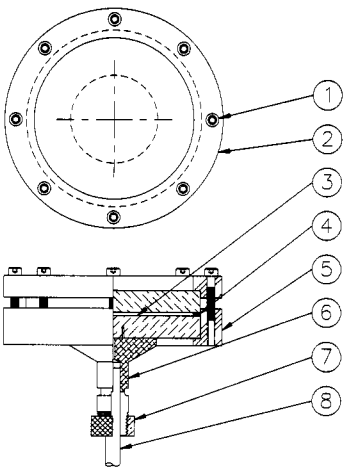

FIGURE 1: Components of centrifugal sample cell: (1) eight 6–32 stainless-steel socket head bolts; (2) phenolic flange; (3) 3-in.-diameter × 3/8th-in.-thick Pyrex disk; (4) 0.5-mm neoprene gasket; (5) phenolic flange; (6) aluminum chuck; (7) knurled brass chuck ring; and (8) 0.25-in.-diameter stainless-steel drive shaft.

MATERIALS AND METHODS

Undegraded 124-kDa phytochrome was isolated and purified from etiolated oat seedling shoots (*Avena sativa* L. cv. Garry oat) according to the method of Chai et al. (1987). The sample was solubilized in 20 mM potassium phosphate buffer solution (pH 7.8) containing 1 mM EDTA and 14 mM β-mercaptoethanol. The specific absorbance ratio SAR = $A(667)/A(280)$ of all samples used in the experiments ranged from ~0.82 to 0.90. Our results are not affected by SAR in this range, and the phytochrome kinetics observed by other groups appear to be independent of its purity (Holzwarth et al., 1984; Ruzsicska et al., 1985). The centrifugal sample cell used in pump–probe experiments (Figure 1) was fashioned from two 7.6-cm-diameter, λ/4 flat Pyrex disks separated by a 0.5-mm-thick neoprene spacer. This assembly was compressed between two phenolic flanges, which were secured by eight 6–32 bolts equally spaced along the periphery of the optical disks. One of the disks was epoxied (*in situ* on a lathe, to ensure concentricity) to an aluminum chuck mounted on a 0.25-in.-diameter 304 stainless-steel shaft. The latter was positioned in two Fafnir FS1KDD7 bearing assemblies separated by 15 cm, and was belt-driven by an Ithaco HMS 220 variable-speed light beam chopper motor. Approximately 0.2–0.3 mL of sample was introduced between the optical flats. The centrifugal forces accompanying cell rotation at high speeds confined the sample to a thin annular region against the inner edge of the neoprene spacer. The focused pump and probe beams (beam waist w_0 ~ 30 μm) intersected at a ~6° angle inside this sample region. To ensure sample recycling to Pr phytochrome between laser exposures, an unfocused 734-nm beam (~1-mm diameter, ~50-mW power) from a cw Ti:sapphire laser traversed the annular sample at a different

point on the circumference. While the presence of the 734-nm beam profoundly influenced some of the observed absorption transients (see below), the angular position (e.g., 90° or 180°) of the recycling beam with respect to the pump/probe beam intersection had no effect. The sample optical density at 667 nm in the rotating cell was typically 0.15.

The lasers and pump–probe apparatus have been described previously by Causgrove et al. (1989). A hybrid mode-locked dye laser (DCM laser dye, DDCI saturable absorber) was pumped with 532-nm SHG pulses (~1-W average power) from a cw mode-locked Nd:YAG laser. Dye laser pulses typically showed autocorrelations with ~2-ps fwhm, and were tunable from 635 to 705 nm. In these one-color pump–probe experiments, an inconel-coated beamsplitter divided the dye laser output into pump and probe beams. Pump–probe signals were detected using an RF multiple modulation scheme; the pump and probe beams were modulated at 6.5 and 0.5 MHz. The 7.0-MHz sum frequency component in the transmitted probe beam was detected using a Drake R-7A narrow-band radio receiver, which converted it into an internal signal-bearing 50-kHz frequency component. The pump polarization could be alternated among parallel, perpendicular, or at a 54.7° angle with respect to the fixed probe polarization. The variable pump pulse time delay was provided by a Micro-Controle UT100125PP translation stage. An EG&G FOD-100 silicon photodiode detected the probe beam. The signal-bearing 50-kHz internal frequency in the radio receiver was routed to a Stanford Research Systems SR510 lock-in amplifier. Time-dependent pump–probe profiles were accumulated in an Electra 486DX computer, and analyzed using a Simplex convolute-and-compare algorithm. All experimental functions (including time delay sweeping, laser beam shutters, data acquisition, and data analysis) were combined in a universal program (SPECTRA) written in Borland C++ language.

The maximum rotational frequency of the ~7.6-cm-diameter sample region was 45 Hz (2700 rpm), yielding a maximum linear speed of 9 m/s for sample travel through the laser beams. For laser beam waist w_0 = 30 μm, this corresponded to a spot turnover frequency $f_s \sim 3 \times 10^5$ s^{-1} (turnover time $1/f_s \sim 3$ μs). At the laser repetition rate f_r = 76 MHz, each sample region was then exposed to f_r/f_s ~250 laser pulses per turnover time. However, the number of chromophores in the beam intersection volume (~8×10^9) exceeded the maximum number of photons absorbed per 40-pJ laser pulse at 667 nm (1×10^7) by a factor of ~800. Hence, at this rotation speed, essentially all of the pump pulses were absorbed by ground-state Pr phytochrome. For wavelengths other than 667 nm, this condition was satisfied *a fortieri*. At significantly slower rotational speeds, artifacts appeared due to excitation of phytochrome intermediates (see below). The sample rotation was supplemented by simultaneous periodic, radial translation over 3 mm at 2 Hz, in order to avoid spatial hole-burning in a single 30-μm annulus.

The pump and probe beam intensities were independently monitored for normalization of time-dependent absorption difference profiles. The pump beam intensity transmitted by the sample was detected with an FOD-100 photodiode and quantified using an analog-to-digital converter (ADC) that communicated with an RS-232 port in the lock-in amplifier. The transmitted pump beam intensity I'_{pump} was related to the incident pump beam intensity I_{pump} by $I'_{pump} = I_{pump}T\kappa(\lambda)$, where T is the static sample transmission and $\kappa(\lambda)$ is the Si photodiode spectral response. [The static transmission is applicable because the laser-induced absorption changes ($\Delta A \sim 10^{-4}$) were negligible compared to the static absorption.] A similar relationship is obeyed by the incident and transmitted probe beam intensities I_{probe} and I'_{probe}. The total signal S' detected by the probe photodiode was $S' = I_{probe}(T + \Delta T)\kappa(\lambda)$, where ΔT is the infinitesimal 7-MHz component that is detected in the radio receiver. The DC component I'_{probe} in S' was monitored with a second ADC. In order to normalize absorption differences obtained at different wavelengths (and hence to generate decay-associated spectra), the absorption differences were normalized to the relative numbers of absorbed photons using

$$\Delta A \propto \frac{ST^2\kappa(\lambda)}{I'_{pump}I'_{probe}(1-T_{0.3})\lambda T_{0.3}} \quad (1)$$

where $T_{0.3}$ is the wavelength-dependent sample transmission for the 0.3-mm beam intersection length and S is the 7-MHz transient absorption signal detected in the radio receiver.

In order to extract optimum resolution of the fastest lifetime components, a laser autocorrelation function (used for data deconvolutions) was obtained *simultaneously* with every pump–probe scan, using a zero-background $LiIO_3$ crystal. This autocorrelation signal was measured and stored in the 486DX computer during runs, using a third ADC.

RESULTS

Time-resolved absorption difference profiles were obtained at 14 wavelengths from 635 to 700 nm. For each profile, the 734-nm Pr recycling beam was either blocked or open, and the cell rotation speed was either fast (9 m/s linear translation speed) or slow (0.4 m/s). All four combinations of these conditions were investigated at most wavelengths. When the 734-nm beam was open, Pr phytochrome strongly dominated the sample absorption spectrum (not shown). When this beam was blocked, the sample contained substantial Pfr as well as Pr phytochrome, in proportions that depended on the pump–probe laser wavelength. [The isosbestic point of the Pr and Pfr absorption spectra (Zhang et al., 1992) occurs at ~690 nm.] At high rotation speed, the absorption transients are dominated by primary excited-state processes resulting from excitation of ground-state Pr phytochrome. At low speed, processes stemming from excitation of intermediates (e.g., lumi-R) become important.

Wavelength Dependence. Magic-angle optical density transients obtained under high rotation speed with the 734-nm recycling beam open are shown in Figure 2 for pump/probe wavelengths 640, 660, and 695 nm. Between 635 and 675 nm, the (negative) absorption difference is dominated by a combination of ground-state photobleaching (PB) and stimulated emission (SE) at all times monitored (out to ~500 ps). At the longer wavelengths (685–700 nm), an initial PB/SE signal is supplanted within several tens of picoseconds by a (positive) absorption signal that persists for times well beyond the 500-ps window. In all cases, the rise time of the initial PB/Si signal is instrument-limited, with an upper limit of conservatively 1–2 ps. Triexponential analyses of these and other profiles are shown Table I. In all triexponential fits, the longest component lifetime, τ_3, was fixed at 100 ns (essentially infinity), in order to simulate nonzero asymptotes, $\Delta A(\infty)$, arising from formation of long-lived intermediates. Two triexponential analyses were performed for each profile: (a) with lifetimes τ_1 and τ_2 freely optimized; (b) with the short-component lifetime τ_1 frozen at 16.5 ps. The final lifetimes τ_1 and τ_2 so obtained are plotted versus wavelength for all experimental runs in Figure 3.

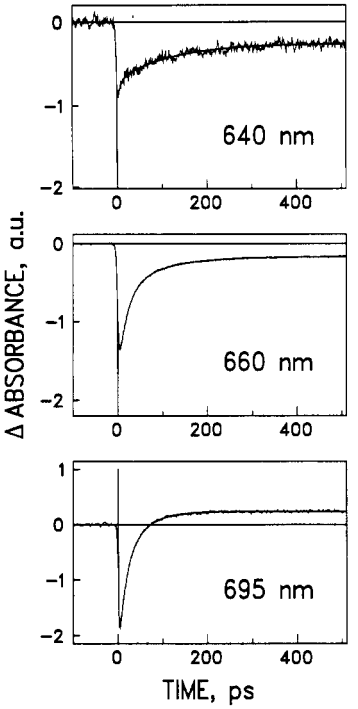

FIGURE 2: Isotropic (magic-angle) absorption difference profiles, $\Delta A(t)$, for native oat phytochrome at 640, 660, and 695 nm. Negative and positive signals correspond to photobleaching/stimulated emission and transient absorption, respectively. Final parameters for biexponential and triexponential fits to these profiles are listed in Table I. Profiles for different wavelengths are not mutually normalized in this figure.

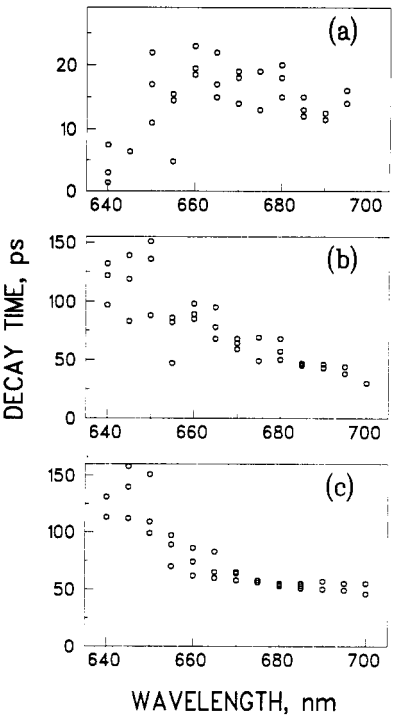

FIGURE 3: Wavelength dependence of optimized lifetimes obtained in triexponential fits to isotropic absorption difference profiles: (a) fast-component lifetimes τ_1 from fits in which τ_1 and τ_2 were freely varied; (b) intermediate-component lifetimes τ_2 from fits in which τ_1 and τ_2 were freely varied; (c) intermediate-component lifetimes τ_2 from fits in which τ_1 was fixed at 16.5 ps.

Table I: Optimized Parameters for Triexponential Fits to Phytochrome Absorption Difference Profiles[a]

	lifetimes τ_1, τ_2 optimized; τ_3 fixed			
λ (nm)	$\tau_1(A_1)$	$\tau_2(A_2)$	$\tau_3(A_3)$	χ^2
640	7.5(–0.38)	132(–0.39)	1 × 10⁵(–0.23)[b]	0.201
645	48(–0.24)	139(–0.32)	1 × 10⁵(–0.44)[b]	0.238
650	22(–0.60)	136(–0.25)	1 × 10⁵(–0.15)[b]	0.233
655	15(–0.55)	82(–0.32)	1 × 10⁵(–0.13)[b]	0.315
660	19(–0.62)	85(–0.28)	1 × 10⁵(–0.10)[b]	0.214
665	19(–0.62)	73(–0.30)	1 × 10⁵(–0.08)[b]	0.398
670	14(–0.58)	59(–0.38)	1 × 10⁵(–0.04)[b]	0.583
675	13(–0.53)	49(–0.44)	1 × 10⁵(–0.03)[b]	0.432
680	15(–0.57)	50(–0.43)	1 × 10⁵(0.01)[b]	0.394
685	15(–0.56)	47(–0.44)	1 × 10⁵(0.03)[b]	0.350
690	17(–0.60)	47(–0.40)	1 × 10⁵(0.09)[b]	0.527
695	14(–0.55)	44(–0.45)	1 × 10⁵(0.09)[b]	0.131
700	3.6(–0.36)	34(–0.64)	1 × 10⁵(0.14)[b]	0.278
	lifetime τ_2 optimized; τ_1 and τ_3 fixed			
λ (nm)	$\tau_1(A_1)$	$\tau_2(A_2)$	$\tau_3(A_3)$	χ^2
635	16.5(–0.15)[b]	264(–0.55)	1 × 10⁵(–0.30)[b]	0.253
640	16.5(–0.15)[b]	113(–0.54)	1 × 10⁵(–0.31)[b]	0.209
645	16.5(–0.15)[b]	112(–0.43)	1 × 10⁵(–0.43)[b]	0.238
650	16.5(–0.52)[b]	99(–0.32)	1 × 10⁵(–0.16)[b]	0.230
655	16.5(–0.57)[b]	89(–0.30)	1 × 10⁵(–0.13)[b]	0.317
660	16.5(–0.57)[b]	74(–0.33)	1 × 10⁵(–0.10)[b]	0.221
665	16.5(–0.57)[b]	65(–0.35)	1 × 10⁵(–0.08)[b]	0.406
670	16.5(–0.63)[b]	65(–0.33)	1 × 10⁵(–0.04)[b]	0.591
675	16.5(–0.63)[b]	58(–0.35)	1 × 10⁵(–0.03)[b]	0.440
680	16.5(–0.63)[b]	54(–0.38)	1 × 10⁵(0.01)[b]	0.389
685	16.5(–0.63)[b]	51(–0.38)	1 × 10⁵(0.03)[b]	0.349
690	16.5(–0.63)[b]	50(–0.37)	1 × 10⁵(0.08)[b]	0.525
695	16.5(–0.65)[b]	49(–0.35)	1 × 10⁵(0.09)[b]	0.131
700	16.5(–0.58)[b]	46(–0.42)	1 × 10⁵(0.18)[b]	0.282

[a] Cell rotation speed, 9 m/s; 734-nm laser power, 120 mW. All lifetimes are in picoseconds. [b] Fixed lifetime parameter.

For wavelengths >665 nm, the optimized short-component lifetimes τ_1 range from 12 to 20 ps, with a mean of ~16 ps (Table I and Figure 3). Their deviations increase considerably toward shorter wavelengths, where the S/N and the short-component amplitude become lower (cf. the 640-nm profile in Figure 2). In these fits, the optimized intermediate component lifetimes τ_2 vary considerably with wavelength even for λ >670 nm; typical τ_2 values are 60–70 ps at 670 nm, and 40–50 ps at 690 ps. Much of this wavelength-skewing in τ_2 for λ >670 nm arises from covariance in the triexponential fits. In separate fits with τ_1 fixed at 16.5 ps (Table I and Figure 3), τ_2 always falls between 50 and 60 ps for 670 nm < λ < 695 nm; the scatter in τ_2 is similarly reduced at other wavelengths. Analogous reductions in scatter are observed in the preexponential factors (not shown). However, the mean τ_2 progressively lengthens to >100 ps as the wavelength is reduced from 670 to 640 nm. This may reflect increased admixtures of a fourth component, with a lifetime similar to that of a 180-ps impurity component reported by Holzwarth et al. (1992).

Decay-Associated Spectra. Wavelength-dependent preexponential factors from triexponential fits with τ_1 fixed at 16.5 ps (Table I) were mutually normalized using eq 1, yielding the decay-associated spectra (DAS) shown in Figure 4. The Pr absorption spectrum used for computation of the static sample transmissions T and $T_{0.3}$ is shown in the top panel of this figure. The short- and intermediate-component DAS (corresponding to lifetimes τ_1 = 16.5 ps and τ_2 = 46–100 ps at most wavelengths) maximize at 690–695 nm, and hence are similar to the absorption spectra of the lumi-R_1/lumi-R_2 intermediates (Zhang et al., 1992). They also resemble (but are slightly red-shifted from) fluorescence DAS for the 6–18- and 46–54-ps Pr* components observed by Holzwarth et al. (1992). Our DAS for the long-component τ_3, shown in the bottom panel, exhibits a (negative) PB/SE band maximum that coincides with that in the Pr ground-state spectrum. It

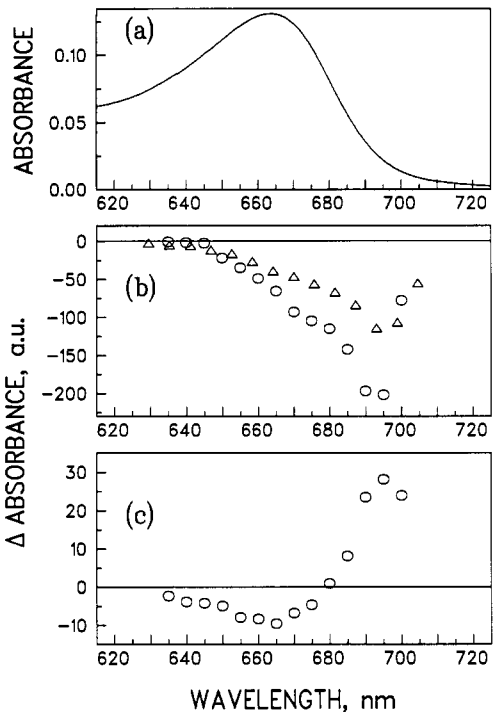

FIGURE 4: Static absorption spectrum of Pr phytochrome (top); decay-associated spectrum for 16.5-ps fast component in triexponential fits to isotropic absorption difference profiles (circles, center); decay-associated spectrum for 40–100-ps intermediate component (triangles, center); and decay-associated spectrum for long component (circles, bottom).

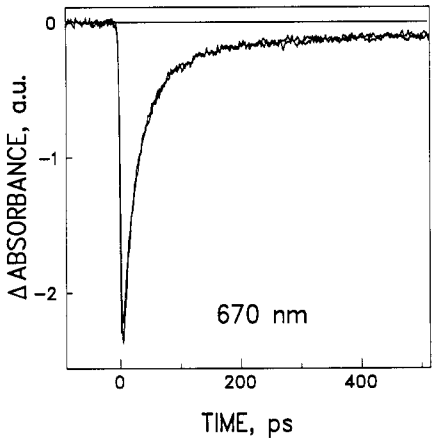

FIGURE 5: Dependence of 665-nm isotropic absorption difference profile on cell rotation speed with 734-nm beam open; rotation speeds of 9 and 0.4 m/s are shown.

also exhibits a positive band maximum at ~690 nm, which resembles the absorption spectra of lumi-R_1 and lumi-R_2.

The DAS displayed in Figure 4 were evaluated from absorption transients generated using a 734-nm Pfr → Pr recycling beam and high cell rotation speeds. In the absence of information concerning steady-state phytochrome equilibria under other experimental conditions (e.g., slow rotation speeds), it is not meaningful to extract DAS from the latter experiments.

Influence of Cell Rotation Speed. The sensitivity of the absorption difference profiles to sample turnover in the presence of the 734-nm Pfr → Pr recycling beam is illustrated in Figure 5, which shows 670-nm magic-angle transients obtained at 9 and 0.4 m/s cell rotation speeds. The actual signal magnitudes (normalized to the product of laser powers in the pump and probe beams) are displayed, so that profiles generated at the two speeds can be directly compared. The

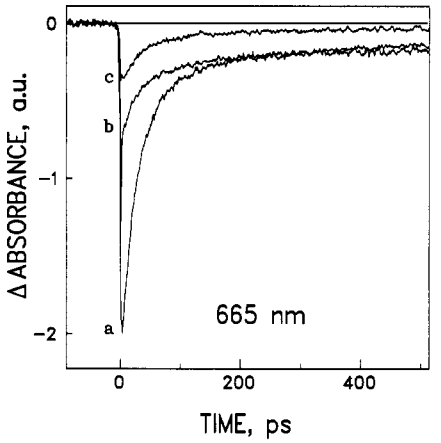

FIGURE 6: 665-nm isotropic absorption difference profiles obtained with (a) 734-nm beam open and 9 m/s cell rotation speed, (b) 734-nm beam blocked and 0.4 m/s cell rotation speed, and (c) 734-nm beam blocked and 9 m/s cell rotation speed.

wavelength 670 nm is close to the isosbestic points between the Pr spectrum and the lumi-$R_{1(2)}$ spectra (Zhang et al., 1992). At cell rotation speeds of 9 and 0.4 m/s, each chromophore is therefore excited ~0.3 and 7 times, respectively, during sample turnover times of ~3 and 70 μs. Nevertheless, the two profiles are nearly *identical* in amplitude and shape; triexponential analyses yield essentially the same lifetime parameters in either case. [This situation contrasts with the profiles obtained when the 734-nm beam is blocked. In this case, very different profiles are obtained at these two speeds (see below), illustrating that the sample turnover time is generally critical.] Further increases in the rotation speed do not appreciably change the observed absorption difference signal. Clearly the excited state(s) responsible for the observed short- and intermediate-component lifetimes can be accessed *immediately* (within 1–2 ps) with large probability, *by exciting phytochrome intermediate(s)* as well as by exciting ground-state Pr.

Influence of 734-nm Laser Power. An example of the sensitivity of the magic-angle absorption transients to the presence of the 734-nm Pfr → Pr recycling beam is given for the pump/probe wavelength 665 nm in Figure 6. At this wavelength, the ratio of absorption coefficients of Pr and Pfr phytochrome is ~2.5:1 (Zhang et al., 1992). The principal effect of blocking the 734-nm beam at high rotation speed is to diminish the entire absorption difference profile (which is dominated by PB/SE at all times), without significantly changing the preexponential factors or lifetimes. The latter are comparatively insensitive to 734-nm power at all of the wavelengths studied; only the scale factor for the entire absorption difference profile is influenced.

The absorption difference profiles become markedly sensitive to the cell rotation speed when the 734-nm beam is blocked, as shown for 665 nm in Figure 6. Here the profile under 0.4 m/s rotation speed differs in shape from the 9 m/s profile, owing to the presence of a 500-ps PB decay component that is absent at the higher rotation speed. Similar lifetime components (520 ps at 655 nm, 720 ps at 645 nm) are found at other wavelengths. These likely arise from intermediate(s) in the reverse (Pfr → Pr) phototransformation, and have not been previously detected.

Anisotropy Decay. A typical 645-nm anisotropy decay is shown in Figure 7 at slow rotation speed, in the absence of the 734-nm recycling beam. Similar anisotropy decays are observed at other wavelengths, and they are little affected by the rotation speed or the recycling beam. The initial anisotropy

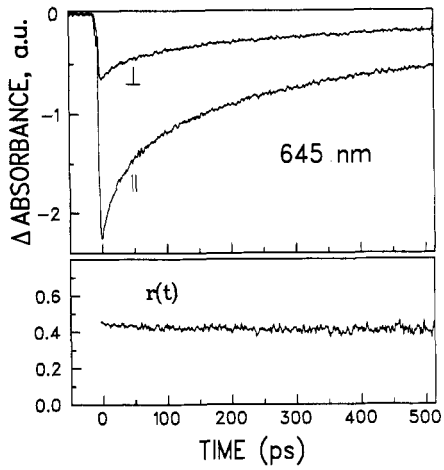

FIGURE 7: Anisotropic absorption difference signals $\Delta A_{\parallel}(t)$ and $\Delta A_{\perp}(t)$ for native oat phytochrome at 645 nm (top); calculated anisotropy function (bottom). Cell rotation speed was 8.0 m/s, laser powers in the 734-nm recycling beam and 645-nm pump beam were 120 and 3 mW, respectively.

$r(0) \sim 0.44$ is slightly above 0.4; $r(t)$ decays slowly (with lifetime conservatively >2 ns) over the next 500 ps. It exhibits no kinetics analogous to the fast or intermediate components in the isotropic decays (Figure 2); no prominent ultrafast component is observed in $r(t)$ with lifetime ≤30 ps. It bears a family resemblance to the fluorescence anisotropy decays observed by Song et al. (1989) for 124-kDa oat phytochrome, except that their initial fluorescence anisotropies were somewhat lower than 0.4.

DISCUSSION

The short- and intermediate-lifetime components (~16 and ~50–60 ps) observed at most wavelengths >665 nm resemble the dominant Pr* fluorescence components observed in recent photon counting experiments (Holzwarth et al., 1992). These components therefore arise from the same primary photoprocesses that are responsible for Pr*-state decay. Our PB/SE kinetics exhibit no discernible rise times at any wavelength under our time resolution of 1–2 ps. Our results differ in this respect from the transient absorption study of Lippitsch et al. (1988). The question arises as to whether our 16- and 50–60-ps "photobleaching decay" components arise principally from (a) *absorption rise kinetics* stemming from creation of the 690-nm lumi-R absorption feature or (b) Pr*-*stimulated emission*. (The latter process inevitably accompanies an absorption difference signal from an optically allowed excited state. In this case, the probe photon stimulates emission of a secondary photon from the Pr* state; the emergent photon exhibits polarization and wavevector that are collinear with those of the probe photon.) Distinguishing these two possibilities in phytochrome is spectroscopically problematic. While the DAS of our short- and intermediate-lifetime components resemble the 690-nm lumi-R absorption spectrum (Zhang et al., 1992), they are also similar to the DAS of the corresponding fluorescence components (Holzwarth et al., 1992). The latter spectra would differ from the expected stimulated emission spectra only by a factor of λ^3. Hence, the observed DAS for these components in Figure 4 are consistent with both interpretations *a priori*.

Our long-component DAS is relevant in this context. This bipolar long-time spectrum, with its photobleaching maximum at 665 nm and lumi-R absorption band at 695 nm, is similar (in band positions and relative amplitudes) to the difference absorption spectrum between lumi-$R_{I(2)}$ and unphotolyzed Pr (Zhang et al., 1992). At early times, the absorption difference signal *in the absence* of stimulated emission is given by

$$\Delta A(0) \propto -\epsilon_{Pr} N_0 x \tag{2}$$

while at long times it will be given by

$$\Delta A(\infty) \propto (\epsilon_{\text{lumi-R}} - \epsilon_{Pr}) N_0 (x - y) \tag{3}$$

Here N_0 is the total phytochrome concentration, x is the fraction of phytochrome initially excited into the Pr* state, and $y \leq x$ is the fraction of phytochrome that reverts to ground-state Pr instead of forming lumi-R. The absorption coefficients of the lumi-$R_{I(2)}$ intermediates are larger than that of Pr phytochrome by a factor of ~2 at 695 nm (Zhang et al., 1992). The expected ratio of absorption differences measured at this wavelength at early and long times is then

$$\frac{|\Delta A(0)|}{|\Delta A(\infty)|} \sim \frac{x}{x - y} \tag{4}$$

The observed ratio is ~10 (cf. the 695-nm absorption difference profile in Figure 2). Equation 4 then implies that 90% of Pr* molecules return to ground-state Pr, which contradicts the report that the quantum yield for Pr ground-state recovery is ~0.5 (Heihoff et al., 1987). Hence, stimulated emission must be a major component in the absorption difference signals displaying picosecond kinetics near 695 nm. The above arguments apply *a fortieri* if the Pr* state exhibits excited-state absorption at this wavelength. The DAS maxima of the short- and intermediate-lifetime components τ_1 and τ_2 (~695 and 690 nm, respectively) appear to be red-shifted by several nanometers from the corresponding fluorescence DAS components (Holzwarth et al., 1992). This is consistent with the fact that the Einstein coefficient A_{21} for spontaneous emission is proportional to ν^3 times the stimulated emission coefficient B_{21}.

The relative insensitivity of the Pr absorption difference profiles to sample turnover times implies that excitation of certain phytochrome intermediate(s) creates a fluorescing chromophore that is kinetically and spectroscopically indistinguishable from that in Pr* phytochrome. These intermediates probably include one or both of lumi-R_1 and lumi-R_2. Hence, an analogous relationship may exist between Pr and lumi-R phytochromes. This would be the case if Pr and lumi-R differed principally in chromophore conformation (e.g., Z,Z,Z versus Z,Z,E; Rüdiger, 1987). The fact that Pr* can be generated instantaneously by light absorption in lumi-R suggests that extensive *protein* conformational changes do not occur in the Pr* → lumi-R conversion.

We next consider the kinetics of lumi-R formation from Pr*. The long-component DAS spectrum (Figure 4) exhibits a well-developed lumi-R absorption band, in addition to the 665-nm Pr photobleaching band. The ratio of their intensities is similar to the ratio of lumi-R absorption and Pr photobleaching features measured at 1 μs (Ruzsicska et al., 1985). Hence, lumi-R formation is certainly complete within several tens of picoseconds. Beyond this, our absorption difference experiments must be interpreted with caution, because the actual lumi-R formation kinetics (signaled by an absorption rise time component) may be masked by the intense Pr*-stimulated emission decay. Since triexponential analyses of our transients at 690–700 nm reveal no components with lifetime >50 ps (aside from the nominal 100-ns component used to simulate the long-time asymptote at these wavelengths), it appears likely that lumi-R is formed directly upon Pr* decay. We do not find evidence for ~40-ps delay between Pr* decay

and lumi-R formation (Lippitsch et al., 1988).

Our time-dependent absorption difference profiles qualitatively resemble those of Kandori et al. (1992). Our data reveal Pr PB/SE kinetics that are not monophasic: for wavelengths >670 nm, triexponential analyses reveal two component lifetimes (~16 and 50–60 ps) similar to those of the major Pr* fluorescence components (Holzwarth et al., 1992). This would be consistent with a Pr* excited-state potential energy surface exhibiting a double minimum along the isomerization reaction coordinate, as proposed by Holzwarth et al. While the 24-ps lifetime measured by Kandori et al. may thus correspond to a weighted average of the two lifetimes τ_1 and τ_2, the results of one-color pump–probe experiments such as ours must be interpreted with caution. Our derivation of DAS from one-color profiles implicitly assumes that the Pr absorption band is spectrally homogeneous and that vibrational thermalization occurs essentially within the laser pulse. In an alternative scenario consistent with our data, the fast component may arise from spectral evolution accompanying vibrational relaxation of Franck–Condon Pr* states (whose nature depends on the excitation wavelength) and/or thermalization of vibrationally hot lumi-R phytochrome formed from the Pr* state. Our transients at shorter wavelengths (645–675 nm) show evidence for the existence of an additional photobleaching decay component, with lifetime >100 ps (Figure 3). This may be due to a Pr ground-state recovery channel, or it may arise from an unknown impurity that is responsible for long-lifetime components in Pr* fluorescence decays (Holtzwarth et al., 1992). At the shortest wavelengths (640–645 nm), a very fast component appears with lifetime <10 ps. Low S/N prevents accurate determination of our short-component lifetimes as these wavelengths, but they may parallel the accelerated fast-component decay found in fluorescences excited at the shorter wavelengths (Holtzwarth et al., 1992).

Our anisotropy functions (Figure 7) show little time evolution at any wavelength over the 500-ps time window. The occurrence of anisotropies slightly larger than 0.4 at early times at several wavelengths suggests that the transition moment for Pr* excited-state absorption may exhibit a component perpendicular to the transition moment for Pr ground-state absorption. Kandori et al. (1992) obtained clear evidence for Pr* excited-state absorption at wavelengths <670 nm. Analysis of absorption difference anisotropies for the chromoprotein stentorin I isolated from the protozoan ciliate *Stentor coeruleus* (S. Savikhin, N. Tao, P.-S. Song, and W. S. Struve, unpublished work) shows that in the presence of ground-state PB/SE combined with perpendicularly polarized excited-state absorption, the initial anisotropy can exhibit values ≥0.4 or ≤–0.2. While the long-time anisotropy is dominated by the Pr* – Pr absorption difference and SE at shorter wavelengths, it bears information about the lumi-R absorption transition moment direction at longer wavelengths (unlike the fluorescence anisotropy). Our anisotropies typically decay to values no lower than 0.35, irrespective of wavelength. The orientations of the Pr and nascent lumi-R absorption transition moments are clearly not separated by a large angle. This is in accord with semiempirical SCF calculations that indicate that the Z,Z,Z → Z,Z,E photoisomerization proposed by Rüdiger (1987) would cause little reorientation of the tetrapyrrole electronic transition moment (Song & Chae, 1979).

ACKNOWLEDGMENT

We are indebted to Mr. Terry Herrman and the Ames Laboratory machine shop for the construction of the centrifugal sample cell.

REFERENCES

Bralavsky, S. E., Matthews, J. J., Herbert, J., DeKok, J., Spruit, C. J. P., & Schaffner, K. (1980) *Photochem. Photobiol. 31*, 417–420.

Brock, H., Ruzsicska, B. P., Arai, T., Schlamann, W., Holzwarth, A. R., Braslavsky, S. E., & Schaffner, K. (1987) *Biochemistry 26*, 1412–1417.

Causgrove, T. P., Yang, S., & Struve, W. S. (1989) *J. Phys. Chem. 93*, 6844–6850.

Chai, Y. G., Singh, B. R., Song, P.-S., Lee, J., & Robinson, G. W. (1987) *Anal. Biochem. 163*, 322–330.

Cordonnier, M.-M., Mathis, P., & Pratt, L. H. (1981) *Photochem. Photobiol. 34*, 733–740.

Cross, D. R., Linschitz, H., Kasche, V., & Tennenbaum, J. (1968) *Proc. Natl. Acad. Sci. U.S.A. 61*, 1095–1101.

Heihoff, K., Braslavsky, S. E., & Schaffner, K. (1987) *Biochemistry 26*, 1422–1427.

Hermann, G., Lippitsch, M. E., Brunner, H., Aussenegg, F. R., & Müller, E. (1990) *Photochem. Photobiol. 52*, 12–18.

Hershey, H. P., Barker, R. F., Idler, K. B., Lissemore, J. L., & Quail, P. H. (1985) *Nucleic Acids Res. 13*, 8543–8559.

Holzwarth, A. R., Wendler, J., Ruzsicska, R. P., Braslavsky, S. E., & Schaffner, K. (1984) *Biochim. Biophys. Acta 791*, 265–273.

Holzwarth, A. R., Venuti, E., Braslavsky, S. E., & Schaffner, K. (1992) *Biochim. Biophys. Acta 1140*, 59–68.

Kandori, H., Yoshihara, K., & Tokutomi, S. (1992) *J. Am. Chem. Soc. 114*, 10958–10959.

Linschitz, H., Kasche, V., Butler, W. L., & Siegelman, H. W. (1966) *J. Biol. Chem. 241*, 3395–3403.

Lippitsch, M. E., Riegler, H., Aussenegg, F. R., Hermann, G., & Müller, E. (1988) *Biochem. Physiol. Pflanz. 183*, 1–6.

Litts, J. C., Kelley, J. M., & Lagarias, J. C. (1983) *J. Biol. Chem. 258*, 11025–11031.

Rüdiger, W., Thümmler, F., Cmiel, E., & Schneider, S. (1983) *Proc. Natl. Acad. Sci. U.S.A. 80*, 6244–6248.

Ruzsicska, B. P., Braslavsky, S. E., & Schaffner, K. (1985) *Photochem. Photobiol. 41*, 681–688.

Shimazaki, Y. Y., Inoue, Y., Yamamoto, K., & Furuya, M. (1980) *Plant Cell Physiol. 21*, 1619–1625.

Song, P.-S., Sarkar, H. K., Kim, I.-S., & Poff, K. L. (1981) *Biochim. Biophys. Acta 635*, 369–382.

Song, P.-S., Tamai, N., & Yamazaki, I. (1986) *Biophys. J. 49*, 645–649.

Song, P.-S., Singh, B. R., Tamai, N., Yamazaki, T., Yamazaki, I., Tokutomi, S., & Furuya, M. (1989) *Biochemistry 28*, 3265–3271.

Wendler, J., Holzwarth, A. R., Braslavsky, S. E., & Schaffner, K. (1984) *Biochim. Biophys. Acta 786*, 213–221.

Zhang, C.-F., Farrens, D. L., Björling, S. C., Song, P.-S., & Kliger, D. S. (1992) *J. Am. Chem. Soc. 114*, 4569–4580.